Fluids on differentiated asteroids: Evidence from phosphates in differentiated meteorites GRA 06128 and GRA 06129

Charles K. SHEARER[1*], Paul V. BURGER[1], James J. PAPIKE[1], Zachary D. SHARP[2], and Kevin D. McKEEGAN[3]

[1]Institute of Meteoritics and Department of Earth and Planetary Sciences, University of New Mexico, Albuquerque, New Mexico 87131, USA
[2]Department of Earth and Planetary Science, University of New Mexico, Albuquerque, New Mexico 87131, USA
[3]University of California Los Angeles, Los Angeles, California 90095–1567, USA
[*]Corresponding author. E-mail: cshearer@unm.edu

Abstract–Paired meteorites Graves Nunatak 06128 and 06129 (GRA) represent an ancient cumulate lithology (4565.9 Ma ± 0.3) containing high abundances of sodic plagioclase. Textures and stable isotope compositions of GRA indicate that superimposed on the igneous lithology is a complex history of subsolidus reequilibration and low-temperature alteration that may have extended over a period of 150 Myr. In GRA, apatite is halogen-rich with Cl between 4.5 and 5.5 wt% and F between 0.3 and 0.9 wt%. The $Cl/(Cl + F + OH)$ ratio of the apatite is between 0.65 and 0.82. The Cl and F are negatively correlated and are heterogeneously distributed in the apatite. Merrillite is low in halogens with substantial Na in the 6-fold coordinated Na-site ($\approx 2.5\%$) and Mg in the smaller octahedral site. The merrillite has a negative Eu anomaly, whereas the apatite has a positive Eu anomaly. The chlorine isotope composition of the bulk GRA leachate is $+1.2\permil$ relative to standard mean ocean chloride (SMOC). Ion microprobe chlorine isotope analyses of the apatite range between -0.5 and $+1.2\permil$. Textural relationships between the merrillite and apatite, and the high-Cl content of the apatite, suggest that the merrillite is magmatic in origin, whereas the apatite is a product of the interaction between merrillite and a Cl-rich fluid. If the replacement of merrillite by apatite occurred at approximately 800 °C, the fluid composition is $f(HCl)/f(H_2O) = 0.0383$ and a HCl molality of 2.13 and $f(HCl)/f(HF) = 50$–100. It is anticipated that the calculated $f(HCl)/f(H_2O)$ and a HCl molality are minimum values due to assumptions made on the OH component in apatite and basing the calculations on the apatite with the lowest X_{Cl}. The bulk $\delta^{37}Cl$ of GRA is a $>2\sigma$ outlier from chondritic meteorites and suggests that parent body processes resulted in fractionation of the Cl isotopes.

INTRODUCTION

Understanding the distribution and behavior of water and other volatiles in the early solar system is important in reconstructing the earliest stages of planetesimal accretion and evolution (e.g., McCord et al. 2006; Médard and Grove 2006; Agee 2008; Moskovitz and Gaidos 2008) and in assessing the potential for the addition of water to the terrestrial planets during late accretion (e.g., Delsemme 2001; Drake and Righter 2002; Drake 2005; McCord et al. 2006; Albarède 2009). Over the last few decades, we have become increasingly aware

of the fundamental role of water on primitive asteroidal bodies (e.g., Zolensky et al. 1999, 2008; Brearley and Jones 1998; Brearley 2006 and references within; Jones et al. 2011). As revealed by studies of chondritic meteorites, aqueous alteration occurs between 0 and 300 °C and commonly involved highly saline solutions (e.g., Brearley 2006; Zolensky et al. 2008). Far less understood is the role of water and volatiles during the initial stages of asteroidal differentiation and magmatism. Generally, magmatism on asteroids is considered "dry." Vesicles in eucrites and aubrites (e.g., Mittlefehldt et al. 1998; McCoy et al. 2006), potential

pyroclastic eruptions on asteroids (Wilson and Keil 1991), and the magmatic evolution of the ureilite parent body (e.g., Mittlefehldt et al. 1998; Goodrich et al. 2007) have all been attributed to volatiles and fluids dominated by CO and/or CO_2. Treiman et al. (2004) concluded that the quartz veinlets in the Serra de Magé eucrite meteorite were deposited from liquid water solutions following most of the asteroidal magmatism and that the water was probably not indigenous to 4 Vesta. Meteorite pairs Graves Nunatak 06128 and 06129 (GRA) have provided a rather unique view of early asteroidal magmatism (Shearer et al. 2008a, 2010a; Day et al. 2009). Preliminary examination of these meteorites revealed the potential release of hydrogen sulfide during handling/heating and rusty to yellow-ocher colored alteration along fractures and mineral surfaces. Although Shearer et al. (2008a, 2010a) suggested that the stable isotopic characteristics of GRA and textural relationships among mineral phases hinted at the interactions between the magmatic mineral assemblage and a fluid phase on the parent body, they were unable to reconstruct the alteration history of these meteorites or decipher the nature of fluids that were active during postmagmatic processes. They did propose that the textural relationships between merrillite and apatite may represent either a late-stage magmatic process or the first stages of interaction between the primary GRA mineral assemblage and a fluid. The intent of this paper is to explore (1) the origin for merrillite–apatite intergrowths in the paired GRA meteorites, (2) the potential for fluids derived from the parent body interacting with the GRA magmatic mineral assemblage, (3) the composition of the fluids, (4) the history of fluid-rock interaction, and (5) the role of fluids during early stages of asteroidal evolution.

MAGMATIC AND POSTMAGMATIC HISTORY OF THE PARENT BODY FOR GRA

Graves Nunatak are a unique pair of meteorites that have been the subject of intense study (Arai et al. 2008; Ash et al. 2008; Shearer et al. 2008a, 2010a; Treiman et al. 2008; Zeigler et al. 2008; Day et al. 2009; Park et al. 2010; Usui et al. 2010). These meteorites contain high abundances of sodic plagioclase, relatively Fe-rich pyroxenes (both low- and high-Ca) and olivine, multiple sulfides, Fe-Ni-metal, two phosphates, ilmenite, and spinel. GRA is not a melt composition as the assemblage represents the accumulation of plagioclase plus the aforementioned phases. Superimposed on this magmatic mineral assemblage are episodes of high-temperature reequilibration and low-temperature alteration. It is likely that the latter is a combination of extraterrestrial and terrestrial processes (Shearer et al. 2010a). Previous studies have reached the following conclusions

concerning the petrogenesis of GRA and the origin and evolution of its parent body:

1. Graves Nunatak represents an early episode of asteroidal magmatism with a crystallization age of 4564.25 ± 0.21 Ma. This magmatic event occurred within a few million years of the formation of the solar system (Shearer et al. 2008a, 2010a).

2. Graves Nunatak records a complex subsolidus history that lasted at least 150 Myr after primary crystallization and accumulation of plagioclase. Disturbed Sm-Nd isotopic system and Ar-Ar measurements have been interpreted as indicating other thermal events that may have occurred even later (Park et al. 2010). The history of GRA, reconstructed from the observations of Shearer et al. (2008a, 2010a), Day et al. (2009), Fernandes and Shearer (2010), and Park et al. (2010), is illustrated in Fig. 1.

3. Although GRA is mineralogically distinct from the brachinites, its parent body was geochemically similar to the brachinite parent body in oxygen isotopic composition, mineral chemistries (Fe/Mn), and age of magmatism (Shearer et al. 2008a, 2010a; Zeigler et al. 2008; Day et al. 2009).

4. In contrast to the magmatism represented by ancient basaltic achondrites (e.g., Howardite-Eucrite-Diogenite meteorite suite), the GRA meteorites appear to represent the crystallization product of a magma produced by low degrees of melting of a unique Na- and volatile-rich parent body rather than high degrees of partial melting of an anhydrous mantle (Arai et al. 2008; Shearer et al. 2008a, 2010a).

5. Although this type of mineral assemblage is fairly rare in the meteorite collection, there are small remnants of similar mineral assemblages in numerous types of meteorites (e.g., ureilites; winonaites; iron meteorites such as IAB, IA, IIE) that suggest that this type of magmatism occurs on other asteroids (Shearer et al. 2010a).

6. Low-temperature alteration is multigenerational and complex. Textural observations and stable isotopic measurements hint at the possibility that terrestrial alteration is superimposed upon a low-temperature alteration mineralogy that originated on the GRA parent body (Shearer et al. 2010a).

ANALYTICAL APPROACH

Backscattered electron (BSE) images and K_α X-ray maps of phosphates in two thin sections of GRA (GRA 06129,23 and GRA 06128,55) were made using the Institute of Meteoritics' JEOL JXA-8200 electron microprobe (EMP) operating at an accelerating voltage

Time before present (m.y.)
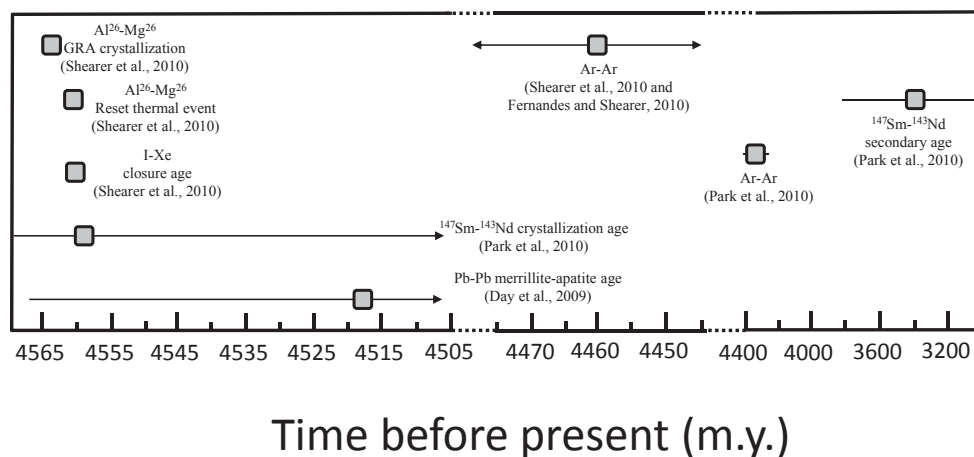
Fig. 1. The isotopic history of GRA as reconstructed from Shearer et al. (2008a, 2010a), Fernandes and Shearer (2010), Day et al. (2009), and Park et al. (2010). Note that the scale bar along the *x*-axis is segmented and the scale of the segment between 3000 and 4400 Myr is different from the other segments. It has been proposed that apatite formation took place anywhere between GRA crystallization at 4564.25 Myr and Sm-Nd isotopic system disruption at approximately 3300 Myr.

15 kV, a beam current of 50 nA, a dwell time of 80 ms, and a resolution of 1 μm per pixel. In particular, K_α (wavelength dispersive X-ray spectroscopy; WDS) X-ray maps for F, Cl, Fe, Na, and Mg were collected on the EMP to explore the distribution of elements between the two phosphates, the chemical heterogeneity of the phosphates, and the potential survivability of magmatic-subsolidus zoning in the phosphates. Following the identification and documentation of phases, samples were repolished and quantitative point analyses were conducted using the JEOL JXA-8200 electron microprobe using a beam current of 20 nA and an approximately 5 μm spot size. Both Cl and F counts were monitored during analysis to account for migration of these two elements during electron beam–sample interactions (Stormer et al. 1993). During most analyses, Cl did not exhibit time-related variability during analysis that was greater than previously documented electron microprobe error for elements of similar concentrations. Where needed, fluorine and chlorine data were extrapolated to time zero to obtain an estimate of the fluorine and chlorine contents. Grains with the steepest and most irregular slopes were discarded from the data set (Stormer et al. 1993). Analyses were standardized using C.M. Taylor Company mineral and metal standards (http://www.2spi.com/catalog/standards/taylor/index.shtml). The accuracy of major element analyses was better than 3%, while the accuracy of minor elements and the halogens was better than 10%. Stoichiometric constraints were used to determine the quality of the data sets, and detection limits were calculated at the 3σ level. Two apatite standards (Taylor, McCubbin) were analyzed during each analytical session. Results of the EMP analyses are presented in Table 1.

The phosphates were analyzed for a suite of trace elements (REE, Sr) following the analytical approach of Shearer et al. (2008b, 2010a) using a Cameca 4f ims ion microprobe. Trace element standards used for these analyses included a well-documented Durango apatite and an apatite standard from Oakridge National Laboratory and the University of New Mexico.

Chlorine isotopes were measured for bulk GRA using the methodology of Sharp et al. (2007) at the University of New Mexico. In this methodology, chlorine is extracted from samples either through leaching in distilled water at room temperature (for leachable Cl), or by melting in a stream of H_2O vapor (pyrohydrolysis) at high temperature (for rock-bound Cl). Chlorine-bearing solutions are reacted with $AgNO_3$, for 24 h, producing AgCl. The dried and filtered AgCl is reacted with excess CH_3I at 80 °C for 2 days to produce CH_3Cl. The CH_3Cl is purified using gas chromatography and analyzed either in dual inlet (standard deviation 0.15‰ 1σ) or in continuous flow (standard deviation 0.4‰ 1σ) gas source mass spectrometry.

Chlorine isotopes were measured on individual apatite grains in GRA using the Cameca ims 1270 ion microprobe at the University of California, Los Angeles. Analyses were performed using a Cs^+ primary beam. Secondary ions of ^{35}Cl and ^{37}Cl were simultaneously collected on electron multipliers. Counting rates ranged from 2×10^5 cps on mass 35 to approximately 7×10^4 cps on mass 37. Five individual chlorine isotope apatite standards were developed at the University of New Mexico for these types of measurements. The major element characteristics of these standards were documented with EMP. These apatite standards had

Table 1. Selected analyses of apatite and merrillite in GRA. Analyses represent individual data points along traverses across apatite and merrillite grains (grain number, point in grain).

Apatite

Analyses by mass	Grain 2 Point 4	Grain 2 Point 17	Grain 3 Point 12	Grain 3 Point 20	Grain 3 Point 29	Grain 4 Point 1	Grain 4 Point 8	Taylor	Taylor[s]	McCubbin	McCubbin[s]
P_2O_5	40.80	41.25	41.03	41.48	41.68	41.18	41.16	40.85	40.93	41.61	41.71
SiO_2	0.02	0.01	0.01	b.d.	0.03	b.d.	b.d.	0.08	0.13	b.d.	b.d.
Ce_2O_3*	0.001	0.001	0.001	0.001	0.001	0.001	0.001	0.36	0.32	0.21	0.12
Y_2O_3	b.d.	b.d.	b.d.	b.d.	b.d.	b.d.	b.d.	b.d.	0.05	0.28	0.24
REE_2O_3*	0.004	0.004	0.004	0.004	0.004	0.004	0.004	n.m.	0.00	n.m.	0.00
Al_2O_3	0.02	0.01	0.02	0.04	0.00	b.d.	b.d.	0.01	0.02	0.01	n.d.
FeO	0.17	0.09	0.18	0.17	0.17	0.19	0.19	0.01	0.06	0.12	0.09
MnO	0.03	0.05	b.d.	0.05	0.03	0.03	0.02	b.d.	0.02	0.68	0.52
MgO	0.03	0.05	b.d.	b.d.	b.d.	0.04	0.01	0.01	0.01	b.d.	b.d.
CaO	53.61	53.62	54.34	54.08	54.02	53.76	53.42	54.39	54.48	54.07	54.24
SrO	b.d.	0.05	b.d.	b.d.	b.d.	b.d.	b.d.	0.37	0.46	b.d.	n.m.
Na_2O	0.45	0.41	0.36	0.42	0.39	0.48	0.40	0.26	0.24	0.15	0.12
SO_3	0.03	0.04	0.04	0.01	b.d.	b.d.	b.d.	0.53	0.65	0.005	n.m.
F	0.71	0.41	0.93	0.89	0.91	0.67	0.67	3.72	3.700	3.90	3.650
Cl	5.02	5.62	4.46	4.76	4.47	5.22	4.94	0.01	0.050	0.003	b.d.
O = F	-0.30	-0.17	-0.39	-0.37	-0.38	-0.28	-0.28	-1.57	-1.56	-1.64	-1.54
O = Cl	-1.13	-1.27	-1.01	-1.07	-1.01	-1.18	-1.11	0.00	-0.01	0.00	0.00
Total	99.44	100.26	99.66	100.46	100.31	100.11	99.42	99.03	99.55	99.40	99.15
Normalized to 8 cations											
Ca	4.935	4.914	4.963	4.928	4.920	4.921	4.921	4.949	4.936	4.9119	4.928
Na	0.075	0.068	0.060	0.069	0.064	0.080	0.067	0.043	0.039	0.0247	0.020
Sr	0.000	0.002	b.d.	0.000	0.000	0.000	0.000	0.018	0.023	0.0000	0.000
Fe	0.012	0.006	0.013	0.012	0.012	0.014	0.014	0.001	0.004	0.0085	0.006
Mn	0.002	0.004	b.d.	0.004	0.002	0.002	0.001	0.000	0.001	0.0488	0.037
Mg	0.004	0.006	b.d.	0.000	0.000	0.005	0.001	0.001	0.000	0.0000	0.000
Al	0.000	0.000	0.000	0.000	0.000	0.000	0.000	0.011	0.010	0.000	0.000
Ce	0.000	0.000	0.000	0.000	0.000	0.000	0.000	0.000	0.002	0.0065	0.004
Y	0.000	0.000	0.000	0.000	0.000	0.000	0.000	0.011	0.000	0.0126	0.011
REE	0.000	0.000	0.000	0.000	0.000	0.000	0.000	0.000	0.000	0.0000	0.000
sum A	5.029	5.001	5.036	5.013	4.998	5.022	5.004	5.023	5.017	5.0130	5.006
P	2.968	2.987	2.961	2.986	2.999	2.978	2.996	2.937	2.930	2.9866	2.994
Si	0.002	0.009	0.001	0.000	0.003	0.000	0.000	0.007	0.011	0.0000	0.000
S	0.002	0.003	0.003	0.001	0.000	0.000	0.000	0.034	0.041	0.0003	0.000
sum B	2.971	2.999	2.964	2.987	3.002	2.978	2.996	2.977	2.983	2.9870	2.994
F	0.193	0.111	0.251	0.239	0.245	0.181	0.182	0.999	0.990	1.0458	0.979
Cl	0.735	0.819	0.648	0.690	0.647	0.760	0.724	0.001	0.007	0.0004	0.000
OH#	0.072	0.070	0.102	0.071	0.108	0.059	0.094	0.000	0.003	0.0000	0.021
sum X	1.000	1.000	1.000	1.000	1.000	1.000	1.000	1.000	1.000	1.0462	1.000
Trace element analyses (in ppm)											
La	5.2	4.6				4.5	6.4				
Ce	11.7	10.5				9.8	14.9				
Nd	8.8	7.9				8.3	13.2				
Sm	2.4	2.2				2.3	3.7				
Eu	2.3	2.2				2.3	2.4				
Dy	3.0	2.7				2.3	4.7				

Merrillite

	Grain 2 Point 9	Grain 2 Point 10	Grain 3 Point 32	Grain 3 Point 36	Grain 3 Point 39	Grain 4 Point 1	Grain 4 Point 8
P_2O_5	46.02	45.74	45.59	45.83	45.83	46.01	45.67
SiO_2	b.d.	b.d.	b.d.	0.01	0.03	b.d.	b.d.
Ce_2O_3*	0.03	0.03	0.03	0.03	0.03	0.03	0.03
Y_2O_3	0.02	0.04	0.03	0.01	0.02	n.m.	n.m.
REE_2O_3*	0.09	0.09	0.09	0.09	0.09	0.09	0.09
Al_2O_3	0.02	b.d.	b.d.	0.03	b.d.	b.d.	b.d.
FeO	1.62	1.48	1.73	1.80	1.83	1.69	1.62
MnO	0.04	0.06	b.d.	0.06	b.d.	b.d.	b.d.
MgO	2.65	2.80	2.59	2.63	2.54	2.68	2.68
CaO	47.15	46.94	46.58	46.80	46.79	46.92	46.78
SrO	b.d.	b.d.	b.d.	b.d.	b.d.	b.d.	b.d.
Na_2O	2.65	2.62	2.43	2.43	2.43	2.59	2.52
SO_3	0.01	b.d.	b.d.	0.002	b.d.	b.d.	b.d.
F	b.d.	b.d.	b.d.	b.d.	b.d.	b.d.	b.d.
Cl	b.d.	0.01	0.007	0.004	0.008	0.01	b.d.
Total	100.29	99.80	99.05	99.68	99.57	100.02	99.39
Normalized to 56 oxygens							
Ca	18.143	18.175	18.132	18.110	18.125	18.087	18.065
Na	1.845	1.836	1.712	1.702	1.703	1.807	1.761
Sr	0.000	0.000	0.000	0.000	0.000	0.000	0.000
Ce	0.004	0.004	0.004	0.004	0.004	0.004	0.004
Y	0.004	0.004	0.004	0.004	0.004	0.004	0.004
REE	0.010	0.010	0.010	0.010	0.010	0.010	0.010
Total	20.006	20.028	19.861	19.829	19.846	19.912	19.844
Fe	0.487	0.447	0.526	0.544	0.553	0.509	0.488
Mn	0.012	0.018	0.000	0.018	0.000	0.000	0.000
Mg	1.419	1.428	1.403	1.416	1.369	1.437	1.440
Al	0.000	0.000	0.000	0.000	0.000	0.000	0.000
Total	1.918	1.893	1.928	1.978	1.922	1.946	1.928
P	13.992	13.994	14.022	14.013	14.027	14.014	14.039
Si	0.000	0.000	0.000	0.000	0.002	0.000	0.000
S	0.000	0.000	0.001	0.001	0.001	0.001	0.001
Total	13.992	13.994	14.023	14.014	14.030	14.015	14.040
Total	35.916	35.916	35.813	35.821	35.799	35.873	35.812
La	80.6	68.5				66.4	67.9
Ce	234.5	199.3				183.9	186.2
Nd	263.0	223.6				194.7	193.7
Sm	75.0	63.8				53.5	52.9
Eu	14.3	12.1				10.0	9.8
Dy	146.6	122.1				102.7	98.3

Table 1. *Continued.* Selected analyses of apatite and merrillite in GRA. Analyses represent individual data points along traverses across apatite and merrillite grains (grain number, point in grain).

Apatite

Analyses by mass	Grain 2 Point 4	Grain 2 Point 17	Grain 3 Point 12	Grain 3 Point 20	Grain 3 Point 29	Grain 4 Point 1	Grain 4 Point 8	Taylor	Taylor[s]	McCunnin	McCunnin[s]
Er	1.5	1.4			1.4	2.7					
Yb	1.3	1.2			1.0	1.8					
Mg#	0.24	0.360	0.000	0.00	0.00	0.27	0.09	0.64	0.23	0.00	0.00
Cl/OH	10.16	11.7	6.37	9.71	5.99	12.82	7.67	9.04	2.24	0.00	0.00
Cl/(OH+Cl+F)	0.73	0.82	0.65	0.69	0.65	0.76	0.72	0.00	0.01	0.00	0.00
Cl/(Cl+F)	0.79	0.88	0.72	0.74	0.73	0.81	0.80	0.00	0.01	0.00	0.00

Merrillite

	Grain 2 Point 9	Grain 2 Point 10	Grain 3 Point 32	Grain 3 Point 36	Grain 3 Point 39	Grain 4 Point 1	Grain 4 Point 8
Er	74.4	62.9				52.6	51.0
Yb	60.4	51.0				42.6	41.1
Mg#	0.744	0.761	0.727	0.723	0.712	0.739	0.747

* estimated from ion microprobe; b.d. = below detection limit; Taylor, McCubbin = measured values of apatite standards; n.m. = not measured; s = documented values of apatite standards; # = OH calculated by difference.

varying amounts of Cl. The chlorine isotopic characteristics of these apatites were documented by the above bulk rock methodology developed by Sharp et al. (2007). The standard (synthetic chloro-apatite from Heidelberg University) and the GRA apatite had similar Cl concentrations. All chloride isotopic compositions determined by mass spectrometry or secondary ion mass spectrometry are standardized relative to SMOC (standard mean ocean chloride, defined as 0‰).

OBSERVATIONS

Textures in Phosphates and Silicates

Two phosphates occur in GRA: a Cl-rich apatite and merrillite. They commonly occur as intergrowths within masses up to 800 μm in length (Figs. 2A–E). In Fig. 2A, the merrillite appears to be partially rimmed by the Cl-apatite with irregular remnants of merrillite enclosed in the apatite. Figures 2B–E further illustrate this relationship with irregular inclusions of merrillite in the apatite or occurring between silicate and apatite grain boundaries. In particular, slivers of merrillite between apatite and olivine are well illustrated in Figs. 2C and 3. These textures suggest that Cl-apatite-forming reactions occur at the expense of merrillite. This relationship between the phosphates is not always as clear. For example, interpretation of the intergrowths presented in Figs. 2D and 3 is ambiguous.

The phosphates do not occur as inclusions in any of the silicates. However, at grain boundaries between the rims of high-Ca pyroxene ($En_{39}Fs_{16}Wo_{45}$ to $En_{44}Fs_{29}Wo_{27}$) and adjacent Cl-apatite, there appear to be reaction boundaries consisting of low-Ca pyroxene ($En_{48}Fs_{47}Wo_5$) with irregular inclusions of high-Ca pyroxene and blebs of sulfides (Figs. 2E and 2F). These low-Ca pyroxene regions between the high-Ca pyroxene and apatite range in thickness between 5 and 20 μm. The low-Ca pyroxene making up this boundary layer between the apatite and high-Ca pyroxene is slightly more Fe- and Ca-rich than the individual orthopyroxenes in GRA ($En_{53}Fs_{45}Wo_2$). Similar textural relationships between apatite and high-Ca pyroxene have been noted in nakhlites (Allan Treiman, personal communication 2010).

Phosphate Compositions

Variations in phosphate composition, structure, and crystal chemistry in extraterrestrial materials have been explored in detail in numerous studies of meteorites and samples collected during the Apollo Program (e.g., Tschermak 1883; Merrill 1915; Mason 1971; Dowty 1977; Delaney et al. 1984; James et al. 1987; Jolliff et al.
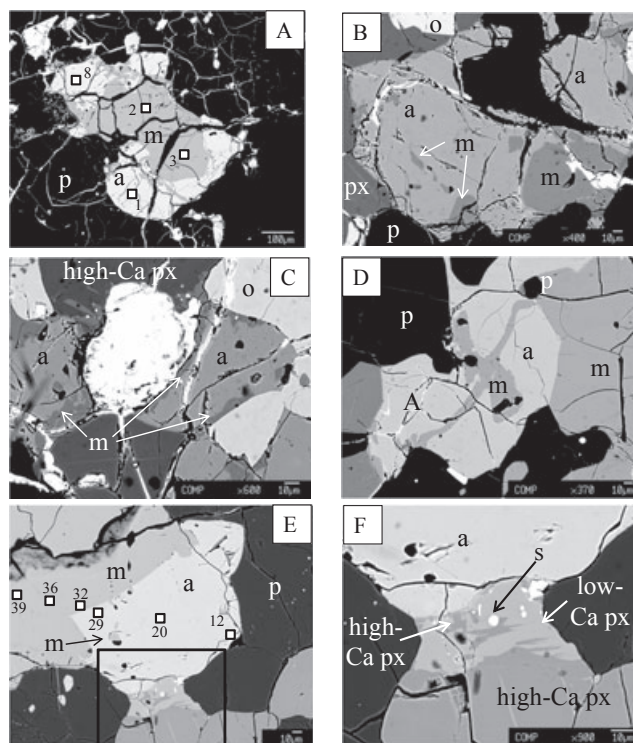
Fig. 2. Backscattered electron images of apatite–merrillite intergrowths. Analytical points in the merrillite and apatite are identified in the images and indexed to Table 1. A) Intergrowth with apatite (a) rimming the merrillite (m). Plagioclase (p) surrounds the phosphate intergrowth. B) Merrillite inclusions in Cl-rich apatite that may illustrate the replacement of merrillite by apatite. Olivine (o) and pyroxene (px) are identified. C) Merrillite along the interface between apatite and olivine. One interpretation of this texture is that the merrillite adjacent to the olivine is partially protected from Reaction 1. D) A much more ambiguous textural relationship between apatite and merrillite. Based on textures alone, the sequence of crystallization is uncertain. E) Relationship among apatite, merrillite, and pyroxene. Apatite appears to irregularly rim the merrillite and merrillite inclusions occur within the apatite. The outlined area is enlarged in (F). F) Replacement of high-Ca pyroxene (px) by low-Ca pyroxene (px) adjacent to apatite interface. Location of this reaction boundary is shown in (E). This texture is very common at the interface between high-Ca pyroxene and apatite. For example, similar textures are also visible in (C) between apatite and high-Ca pyroxene. Sulfide inclusions (s) are very common in this reaction texture.

1993, 2006; Hughes et al. 2006; McCubbin and Nekvasil 2008). The ideal formula for apatite is $Ca_5(PO_4)_3(OH, F, Cl)$. In this formula, phosphorous occurs in tetrahedral coordination, whereas the Ca ions occur in two polyhedra: Ca1 coordinated to nine oxygens and Ca2 coordinated to 6 oxygens and one anion such as Cl, F, OH (Hughes and Rakovan 2002). Merrillite (ideal formula of $Ca_{18}Na_2Mg_2(PO_4)_{14}$ has been referred to in previous literature as "whitlockite" ($Ca_{18}Mg_2(PO_4)_{12}[PO_3(OH)]_2$). In endmember whitlockite, hydrogen is an

essential component forming $PO_3(OH)$ groups, whereas endmember merrillite is devoid of hydrogen and thus $PO_3(OH)$ groups are absent in the structure (Hughes et al. 2006, 2008; Jolliff et al. 2006). Merrillite and whitlockite can form a solid solution (Hughes et al. 2006), but most extraterrestrial samples are often compositionally closer to the merrillite endmember. Halogens within extraterrestrial merrillite have been reported, but are generally in trace abundance and can be difficult to analyze (Greenwood et al. 2003; Jolliff et al. 2006). Jolliff et al. (2006) distinguished among different extraterrestrial merrillite compositions and explored the influence of composition on structure. The merrillite structure consists of three symmetrically different P tetrahedra (14 sites per 56 O atoms); the main 8-coordinated Ca sites are referred to as Ca1, Ca2, and Ca3 (18 sites per 56 O atoms), irregular octahedra sites that accommodate Na (2 sites per 56 O atoms), and smaller octahedral sites referred to as "Mg-site" (2 sites per 56 O atoms). Hughes et al. (2006), Jolliff et al. (2006), and Shearer et al. (2011) discussed the potential element substitutions within these sites.

Examples of apatite and merrillite analyses are presented in Table 1. The location of these analyses is shown in Figs. 2 and 3. Formulae for apatite and merrillite are calculated based on 8 cations and 56 oxygen, respectively. Apatite is halogen-rich with Cl between 4.5 and 5.5 wt% and F between 0.3 and 0.9 wt%. Endmember Cl-apatite contains approximately 6.7% Cl. The distribution of Cl and F within the phosphates is illustrated in Fig. 3. The Cl and F are negatively correlated and are heterogeneously distributed in the apatite. The distribution of F and Cl in apatite is generally patchy in nature (Figs. 3D and 3E), although other apatite grains in GRA exhibit a varying distribution of F-Cl ranging from grains with Cl-rich cores, to grains with Cl-rich rims, to others that appear relatively homogeneous. This patchy texture in apatite from GRA is unlike the concentric zoning often observed in igneous rocks (e.g., Shore and Fowler 1996 and references within; Tepper and Kuehner 1999). However, the patchy distribution of Cl and F in apatite is also fairly common and has been documented by Harlov et al. (2006; see their fig. 1 in crustal xenoliths), Boudreau and McCallum (1992) in the Stillwater Complex, and Jolliff et al. (1989) in a granitic pegmatite in the Black Hills of South Dakota. Water content of the apatite and the merrillite was not determined directly in this study. However, based on the halogen content and apatite stoichiometry, the apatite has only a minor OH component. The $(OH/(OH + Cl + F)$ in the apatite is less than 11%. This is a maximum value for OH as there can be unmeasured components such as oxy- and carbonate-components and vacancies in this site. Within
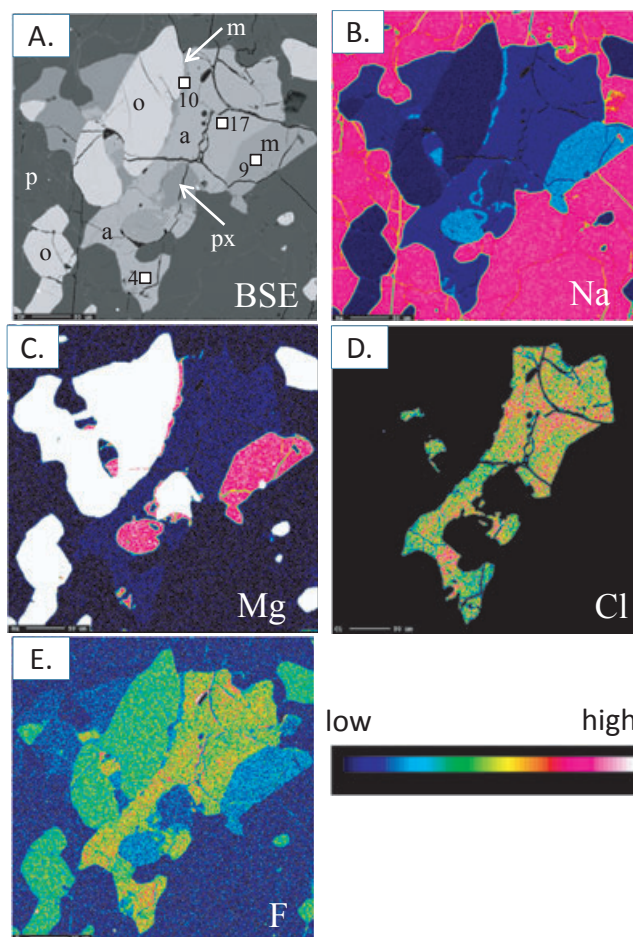
Fig. 3. Backscatter electron (BSE) image and WDS X-ray maps illustrating the textural relationships and elemental distribution between phosphates. A) BSE image illustrating inclusions of merrillite (m) within apatite (a) and between apatite-olivine (o) interface. Pyroxene (px) is shown to be partially to totally enveloped by apatite. Locations of analyses in Table 1 are illustrated. B) Sodium X-ray map of BSE image in 3A. C) Magnesium X-ray map of BSE image in (A). The sodium and magnesium X-ray maps illustrate the enrichment of these elements in merrillite relative to adjacent apatite. D) Chlorine X-ray map of BSE image in (A). E) Fluorine X-ray map of BSE image in (A). Although the negative correlation between Cl and F in the apatite is correct (based on quantitative microprobe analyses), it is very likely that the X-ray flux at the energy of the F Kα includes Fe Lα emissions. The apparent difference in F among the silicates is most likely a result of these combined emissions. Warmer colors in the X-ray maps represent higher X-ray intensities. See color bar for relationship between color and relative intensity.

a Cl-F-OH ternary plot, the apatite plots near the Cl apex (Fig. 4).

Sodium in the apatite ranges from 0.35 to 0.50 wt% Na_2O. The sodium should occupy the Ca site and its substitution for Ca requires a coupled substitution to maintain charge balance. This concentration is significantly
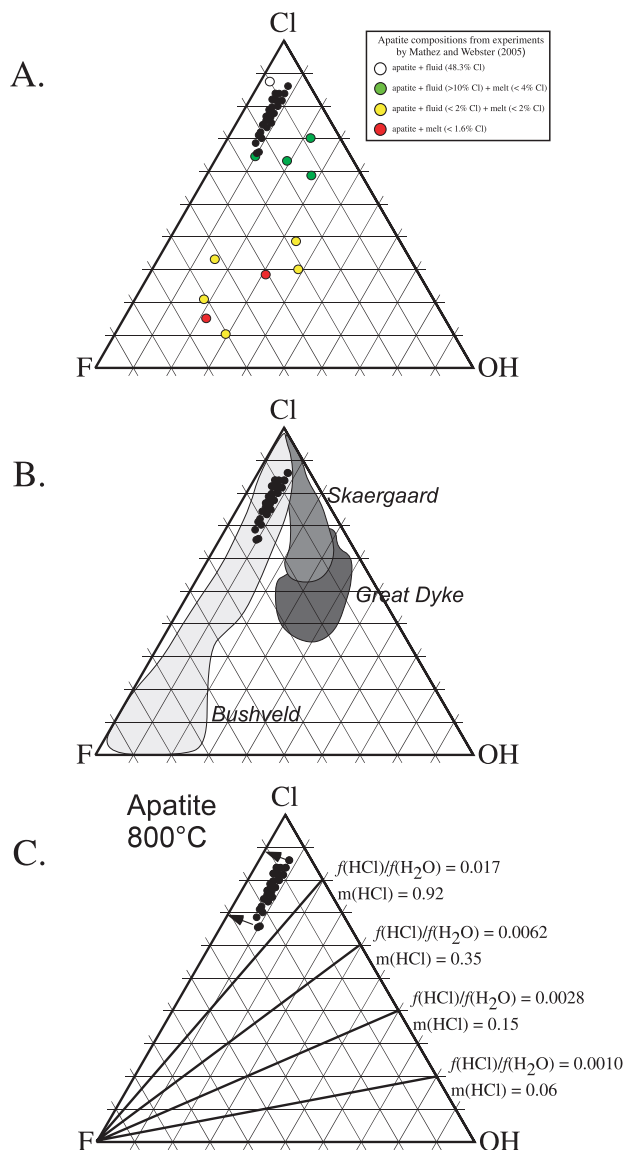
Fig. 4. Apatite compositions and relationship to fluid composition. A) Ternary plot of Cl-F-OH in apatite from GRA. These data are compared with apatite compositions from experiments (from Table 2) of Mathez and Webster (2005). Symbols representing apatite, fluid and melt compositions from these experiments are inserted into the diagram. B) Composition of apatite documented from the Great Dyke, Bushveld, and Skaergaard (Boudreau et al. 1986; Boudreau and McCallum 1992; Boudreau 1993; Meurer and Boudreau 1996). C) Compositional fields in which apatite would form for specific fluid compositions at 800 °C (modified after Piccoli and Candela 2002).

higher than that observed in terrestrial apatite associated with basaltic-intermediate-felsic rocks (Piccoli and Candela 2002). These high Na_2O concentrations in the GRA apatite are similar to apatite in carbonatites, hydrothermally altered rocks (Piccoli and Candela 2002),

and intergrown with merrillite in the Zag H Chondrite (Jones et al. 2011).

Halogens (F and Cl) were not detected in merrillite by electron microprobe (Table 1) although the F X-ray maps in Fig. 3E exhibit some contrast in the distribution of F between merrillite and adjacent silicates. It appears as if the F content of merrillite is higher than plagioclase and pyroxene, yet lower than adjacent olivine. Our microprobe analyses cannot confirm if this difference in F in the X-ray maps is correct. Most likely, the subtle differences in F among merrillite and the silicates in the X-ray map are related to differences in matrices that result in the influence of Fe L_α peak on the measurement of F. In studies of lunar merrillite, Jolliff et al. (1993, 2006) did observe that F in merrillite ranged from below detection limit to 0.6% and probably exceeded the concentration of F in the adjacent silicates. Merrillite in GRA has substantial Na (Na $\approx$ 2.5 wt%) and Mg. As illustrated in Figs. 3B and 3C and Table 1, the merrillite is enriched in Mg, Fe, and Na relative to the apatite. The Mg/Mg + Fe (Mg#) of the merrillite is greater than that of the apatite. The differences in the Mg# are a result of the contrasting geometries of sites in the apatite and merrillite and should not be confused with differences in melt composition or the crystallization sequence of the phosphates (Jolliff et al. 1993). In merrillite, the smaller Mg is preferred due to the presence of the smaller octahedral site. In apatite, the substitution of Fe^{2+} and Mg must occur in the larger seven- to nine-coordinated Ca site. This results in Fe^{2+} being preferred to Mg in apatite and both Fe^{2+} and Mg being preferred in the merrillite structure. Hess et al. (1990) demonstrated experimentally that whitlockite had substantially higher Mg# than its equilibrium melt and proposed that apatite would have a Mg# similar to its equilibrium melt.

The rare earth elements (REE) will occupy the Ca-sites in both apatite and merrillite. Charge balance mechanisms need to accommodate trivalent cations for divalent Ca in the structures of both minerals, and have been discussed in detail by Jolliff et al. (1993, 2006). The REE pattern of the Cl-apatite is slightly light REE-enriched ($\approx$ 10–15 × CI) relative to heavy REE ($\approx$ 6–10 × CI) with a rather uncharacteristic positive Eu anomaly (Fig. 5). The positive Eu anomaly contrasts with REE patterns measured for most extraterrestrial apatite and predicted apatite/melt—apatite/merrillite distribution coefficients (Jolliff et al. 1993). The merrillite is at least 12.5 times more enriched in REE as compared with apatite. The merrillite pattern is enriched in middle REE compared to both light REE and heavy REE, and has a negative Eu anomaly (Fig. 5). The bulk REE pattern of GRA is primarily a product of the REE in phosphates and plagioclase.
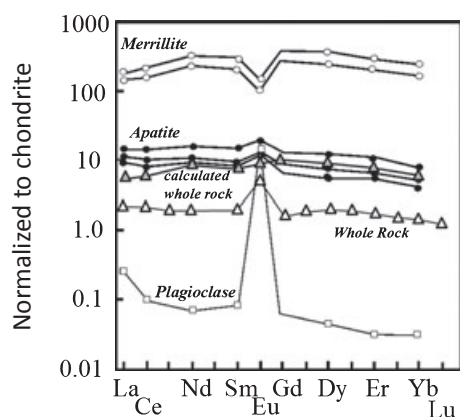
Fig. 5. Rare earth element patterns of merrillite, apatite, and plagioclase from GRA 06129 (modified after Shearer et al. 2010a). Included in the figure is the whole rock REE pattern for GRA 06129 (Shearer et al. 2010a) along with a calculated whole rock GRA 06129 pattern assuming 5% merrillite, 0% apatite, and 95% plagioclase. REE data normalized to Anders and Grevesse (1989).

Fig. 6. Chlorine isotopic composition of chondritic meteorites, bulk GRA, and apatite from GRA 06129. Shaded field outlines the field for the chlorine isotopic composition of terrestrial materials (from Sharp et al. 2007).

Cl-Isotope Composition of GRA 06129 and Phosphates

Chlorine consists of two stable isotopes: ^{35}Cl, which makes up 75.77% of Cl and ^{37}Cl, which makes up 24.23% of stable Cl. $^{36}Chlorine$ exists, but is a product of cosmogenic or anthropogenic processes. The isotopic composition of Cl is represented as $\delta^{37}Cl = (R_{sample}/R_{standard} - 1) \times 1000$ where $R_{sample} = {}^{37}Cl/^{35}Cl$ for sample and $R_{standard} = {}^{37}Cl/^{35}Cl$ for Standard Mean Ocean Chloride (SMOC). The bulk $\delta^{37}Cl$ composition of many primitive meteorites (CI, CM, CV chondrites) is approximately 0‰ (Sharp et al. 2007; Mercer et al. 2011). CAI inclusions (sodalite) have an isotopic composition of $\delta^{37}Cl$ between 0 and −2 (Sharp et al. 2007). The chlorine isotopic composition of the bulk GRA leachate is +1.2‰. The leachate contained 66 ppm Cl. The chlorine isotopic composition of the apatite from ion microprobe measurements ranges from −0.5 to +1.2‰ (Fig. 6).

DISCUSSION

Interpretation of Textures

There are numerous textural relationships between apatite and merrillite and between the phosphates and silicates that give clues to the petrogenesis of the phosphates in GRA (Figs. 2 and 3). Although our interpretation of the apatite-merrillite intergrowths based solely on texture is that Cl-apatite followed the crystallization of silicates and merrillite in the petrogenesis of GRA, there is some ambiguity in this interpretation. For example, Fig. 7 illustrates the contrasting

interpretations for the origin of these phosphate intergrowths. In the petrogenetic sequence shown in Fig. 7A, merrillite is a magmatic phase that predates the crystallization of Cl-apatite. In many lunar and Martian basalts, merrillite is a common magmatic accessory phase and will crystallize prior to apatite (Jolliff et al. 1993, 2006; McCubbin et al. 2011). Chlorine-apatite follows the crystallization of merrillite through the interaction of merrillite with Cl-rich residual melt, fluid, or mesostasis. Within the context of this interpretation, inclusions of merrillite in apatite and at the interface between silicates and apatite, represent remnants of consumed merrillite. Within the context of the model in Fig. 7A, some of the ambiguous phosphates in GRA (Figs. 2D and 2E) can be rationalized by the experimental studies of fluid–phosphate interactions conducted by Harlov et al. (2002). They produced phosphate textures similar to the ambiguous textures observed in GRA and attributed some of this ambiguity to metasomatism along cracks or cleavage planes in the phosphates (see their Figs. 6b and 11). An alternative interpretation of this texture is illustrated in the sequence of petrogenetic images designated in Fig. 7B. In this scenario, Cl-apatite represents the primary phosphate that either crystallized from a late-stage melt or fluid. Merrillite is replacing the Cl-apatite in the solid state following metamorphism related to either shock and/or heating. In this scenario, the merrillite inclusions and merrillite along phase boundaries represent breakdown products of Cl loss by the apatite. A third interpretation of these intergrowths, not shown in Fig. 7, is that merrillite and Cl-apatite cocrystallized from the magma responsible for GRA. Jolliff et al. (1993)
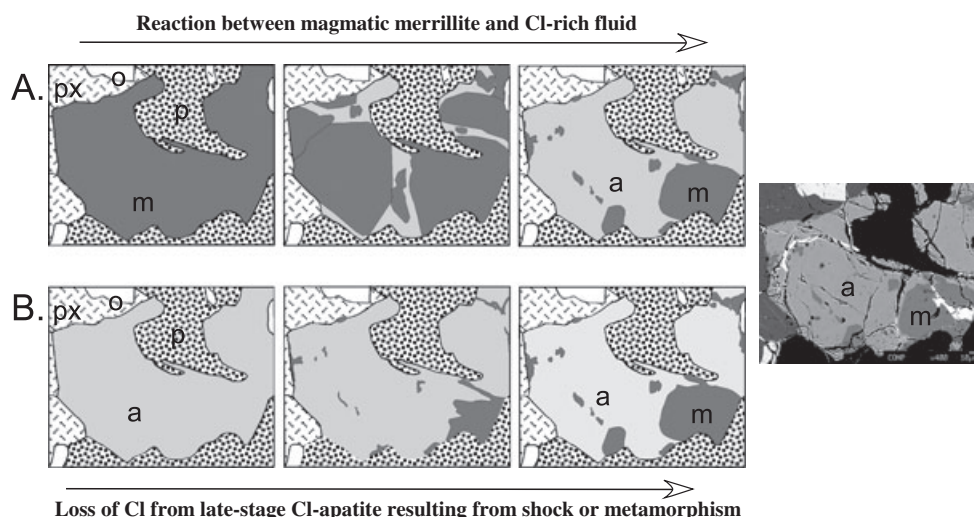
Fig. 7. Two contrasting interpretations of Cl-apatite (=a) and merrillite (=m) intergrowth textures (px = pyroxene, p = plagioclase, o = olivine). A) Merrillite is a primary magmatic phase that is replaced by Cl-apatite through the interaction with Cl-rich fluid derived from either the crystallized GRA magma or the GRA parent body. B) Cl-apatite is a magmatic phase derived from the GRA magma or a postmagmatic phase derived from exsolved magmatic fluids. Shock or metamorphism resulted in halogen and OH loss from the apatite resulting in formation of nonmagmatic merrillite.

documented intergrowths of merrillite and F-apatite in several lunar rocks, which they interpreted as magmatic in origin. The validity of each of these textural interpretations can be evaluated by integrating textural with additional observations and previous studies.

Jolliff et al. (1993) and McCubbin et al. (2011) concluded that the phosphate igneous crystallization sequence is related to the P to F ratio of the melt. The relationship of the P/F ratio to the sequence of phosphate crystallization is illustrated by lunar basalts. McCubbin et al. (2011) concluded that the fluorine content of mare basalt residual melts ranged from 0.79 to 1.11 wt% at the time of apatite crystallization. Lunar basalts often reach phosphate saturation before significant fluorine has built up in the melt to stabilize apatite. This results in the early crystallization of merrillite relative to apatite in many mare basalts. In those lunar magmatic systems in which merrillite and F-apatite are intergrown, it is possible that the ratio of F to P enables the nearly simultaneous crystallization of these two phosphates. The relationship between P/F ratio and the sequence of phosphate crystallization observed in mare basalts may be applicable to GRA. Based on bulk compositions of GRA, individual mineral chemistries, and model abundance of phases (Shearer et al. 2008a, 2010a), the parental melt for GRA had a relatively high P/F ratio that would be favorable for the crystallization of merrillite prior to apatite. Furthermore, numerous studies (Boudreau et al. 1986; Boudreau and McCallum 1989, 1992; Boudreau 1993; Piccoli and Candela 2002; Mathez and Webster 2005; McCubbin

et al. 2011) have concluded that Cl-apatite of compositions similar to those documented in GRA are a product of subsolidus crystallization from a fluid phase. Therefore, magmatic merrillite in GRA must predate the crystallization of Cl-apatite.

In Fig. 7B, intergrowths between the phosphates are the result of postmagmatic Cl-apatite reacting to merrillite as a result of almost total Cl loss from the monovalent site due to the shock or metamorphic processes. Shock and associated thermal metamorphic processes are clearly recorded in the textures and silicate compositions (i.e., heterogeneous, granoblastic texture, exsolution textures, homogeneous mineral compositions) of GRA (Shearer et al. 2008a, 2010a). This appears to be an unlikely reaction to explain the phosphate intergrowths. As demonstrated by Boctor et al. (2003) and McCubbin and Nekvasil (2008), apatite with a fully occupied monovalent ion site exists within maskelynite in the Martian meteorite Chassigny. There is no evidence for the formation of merrillite at these shock conditions. Nyquist et al. (2001) estimated that Chassigny recorded shock pressures of 3.5 GPa. This is a significantly higher shock pressure than was experienced by GRA. It was probably exposed to shock pressures of far less than 3.0 GPa based on the stability of plagioclase instead of maskelynite (e.g., Milton and Decarli 1963; Stöffler 1984). This indicates that a Cl-apatite $\Rightarrow$ merrillite reaction does not occur at shock conditions experienced by GRA.

If our interpretation of the intergrowths between apatite and merrillite is correct, the late-stage of

replacement of merrillite and high-Ca clinopyroxene may be a product of (1) a reaction between a Cl-rich residual melt and earlier magmatic phases, (2) a reaction between Cl-rich, late-stage mesostasis and earlier magmatic phases during subsolidus reequilibration, or (3) a reaction between a Cl-rich fluid and magmatic phases. In scenario (3), the Cl-rich fluid may be exsolved from the GRA parent magma or produced elsewhere in the GRA parent body and is generally unrelated to magmatism that produced the high temperature assemblage in GRA.

Interpretation of Cl Isotopic Composition of GRA

The $\delta^{37}Cl$ value of the Earth is not certain, but it is close to 0.0‰ (Sharp et al. 2007, 2009). The range of Cl isotopic compositions for terrestrial materials is small, and there are few mechanisms on Earth that can result in large isotopic fractionations. Two factors that control Cl isotope fractionation during volatilization on Earth are preferential loss of ^{35}Cl to the vapor phase due to its higher translational velocities, and vapor pressure and the preferential incorporation of ^{37}Cl into HCl (gas) due to the covalent character of the bond. Generally, on Earth, these two counteracting factors mitigate one another, resulting in a near-zero fractionation between magma and vapor (Sharp et al. 2009, 2010). However, in planetary environments in which magmas are significantly lower in H compared with Earth, such as the Moon, factor 2 will be a less important resulting in the enrichment of a vapor phase in light Cl and the enrichment of basaltic magmas in heavy Cl. Sharp et al. (2010) and Shearer et al. (2010b) demonstrated that this fractionation occurred during lunar volcanism.

Like Earth, chlorine isotope compositions for primitive meteorites are fairly limited (Fig. 6). The average of all carbonaceous chondrites is 0.0 ± 0.7‰ (1σ). The bulk $\delta^{37}Cl$ composition of many of the CI, CM, CV chondrites ranges from approximately −0.6 to 0‰ (Sharp et al. 2007). C3 chondrites are all within 0.2‰ of −0.5‰ (Mercer et al. 2011). These measurements led Mercer et al. (2011) to propose that the $\delta^{37}Cl$ value for the solar nebula in the C chondrite-forming region was −0.5‰. The $\delta^{37}Cl$ values for sodalite within CAI inclusions have an average of −1.3‰ (±0.6‰, 1σ), statistically lighter than bulk meteorite data (Sharp et al. 2007). Sharp et al. (2007) concluded that the low values of the sodalite, compared with bulk chondrites, may represent either a second nebular Cl reservoir or equilibrium fractionation of Cl isotopes. They determined that at 825 °C, the 1000 ln $\alpha_{sodalite-NaCl}$ value is −0.3 ± 0.1‰ (1σ) and should increase with decreasing temperature. Therefore, fractionations of −1‰ at lower temperature are reasonable, and could account for the differences between sodalite and the bulk meteorite.

The chlorine composition of bulk GRA (+1.2‰) is more than 2σ distance from the mean value for carbonaceous chondrites. Based on the conclusions reached by Sharp et al. (2007), this difference is not a product of nebular heterogeneity, but more likely a product of Cl isotopic fractionation on the parent body. There are several processes that are capable of producing fractionations on the scale of +1‰ at subsolidus conditions. On the basis of a series of experiments, Sharp et al. (2009) illustrated that in HCl-rich systems, the Cl isotopic composition could be modified by several processes (1) sub-boiling equilibration between aqueous chloride and HCl gas, which has a 1000 ln $\alpha_{HCl(g)-Cl^-}$ = 1.4 to 1.8‰, (2) evaporation of HCl(g) from hydrochloric acid at room temperature, which has fractionation in the opposite sense, with a 1000 ln $\alpha_{HCl(g)-Cl^-}$ = −3.92‰ and (3) a distillation process in which ^{37}Cl-enriched HCl(g) is stripped from the hydrochloric acid resulting in large positive fractionations. These studies suggest that the small Cl isotopic fractionation observed in GRA may reflect the activity of a relatively HCl-rich system on the GRA parent body. It appears unlikely that the Cl isotope composition could result from fractionations between silicate melt and a saline solution or between Cl-rich apatite and a saline solution. Most likely, such processes would cause relatively low fractionation (<<1‰) at near solidus conditions (Sharp et al. 2007, 2009, 2010). However, neither the 1000 ln $\alpha_{apatite-Cl(aq)}$ nor 1000 ln $\alpha_{silicate\ melt-Cl(aq)}$ has been determined for these two processes. Alternatively, the Cl composition does not reflect any processes directly recorded in GRA (e.g., magmatic, phase exsolution, shock, metamorphism). Rather, the extent of Cl fractionation reflects the isotope composition of a chloride-rich fluid phase that was transported into the GRA system after experiencing isotopic fractionation via equilibration between aqueous chloride and either an HCl gas or metal chlorites (Sharp et al. 2010).

Late-Magmatic to Postmagmatic Processes in GRA

The preceding textural interpretation was that the merrillite-Cl-apatite intergrowths are a product of the reaction between merrillite and a late-stage Cl-rich component. This could reflect the interaction between merrillite and either residual Cl-rich melt, -mesostasis, or -fluid.

Residual Melt
Could these textures be a product of the interaction between merrillite and a late-stage residual Cl-rich melt?
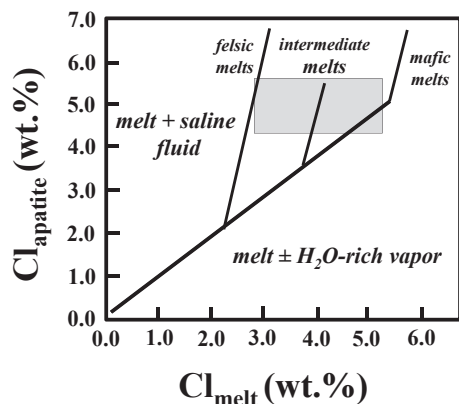
Fig. 8. Cl partitioning among apatite, melt (felsic to basaltic), and saline fluid (modified after Mathez and Webster 2005).

Composite apatite–merrillite intergrowths have been identified in relatively volatile-poor lunar samples, although the apatite in these intergrowths is F-rich and not Cl-rich apatite (Jolliff et al. 1993). In lunar basalts, apatite with intermediate abundances of Cl (Cl = 1–3 wt%) is associated with KREEP basaltic lithologies such as KREEP basalts, highlands magnesian suite and alkali suite (Jolliff et al. 1993; Sharp et al. 2010; Shearer et al. 2010b), whereas high-Cl apatite (Cl = 4–5 wt%) occurs along walls of vesicles in mare basalts and impact produced rocks (Jolliff et al. 1993; Shearer et al. 2010b). Experimental studies of Mathez and Webster (2005) on partitioning of Cl among silicate melt-apatite-fluid shed some light on the origin of Cl-apatite in GRA. Several conclusions may be extracted from Fig. 8 (modified from Mathez and Webster 2005). With crystallization of non-Cl-bearing phases such as the silicates that dominate the GRA mineralogy, the Cl content of the melt will increase. For felsic melts, the Cl content in the melt will reach a maximum of approximately 2% (Mathez and Webster 2005). Apatite that crystallizes from this melt will have a Cl content of approximately 2%. At higher concentrations of Cl, behavior of CI is dependent upon partitioning among a melt-exsolved saline fluid-apatite. The behavior of Cl is very sensitive to melt composition. Clearly, the concentration of Ca and P and the P/F ratio will influence the crystallization of phosphates and the behavior of Cl. For basaltic melts, the saturation point is at significantly higher Cl (approximately 5% Cl) (Mathez and Webster 2005). These data indicate that it would be unlikely for the Cl-apatites observed in GRA to crystallize from the potential range of melt compositions suggested for producing the GRA mineral assemblage (Arai et al. 2008; Ash et al. 2008; Day et al. 2009; Shearer et al. 2010a; Usui et al. 2010).

Metamorphism

Clearly, GRA has been subjected to several stages of shock and metamorphism (Arai et al. 2008; Ash et al. 2008; Shearer et al. 2008a, 2010a; Treiman et al. 2008; Zeigler et al. 2008; Day et al. 2009). Another possible model for late-stage apatite formation is that during subsolidus reequilibration, a late-stage Cl-rich mesostasis could have interacted with the merrillite to produce the Cl-apatite. This model appears unlikely under most scenarios. First, it is difficult to form a Cl-rich mesostasis because as shown in Fig. 8, at relatively low Cl concentrations, the exsolution of a saline fluid would eventually remove the Cl from the late-stage melt (Mathez and Webster 2005). An exception to this might be the precipitation of chlorides in the mesostasis during low-pressure boiling and vapor loss because of the low-water content of the late-stage melt. Second, these is no textural evidence for the existence of a Cl-rich mesostasis in GRA (Arai et al. 2008; Ash et al. 2008; Shearer et al. 2008a, 2010a; Treiman et al. 2008; Zeigler et al. 2008; Day et al. 2009). One could argue that such a mesostasis was not preserved due to metamorphism and shock, but still there is no evidence for its existence in this cumulate textured rock.

Cl-rich Fluid

The experimental data of Mathez and Webster (2005) is most consistent with the Cl-rich apatite in GRA being a product of the interaction between a saline fluid and magmatic merrillite. In their experiments, Mathez and Webster (2005) documented that most Cl-rich apatites coexisted with either silicate melt and a high-Cl fluid (Cl ≈ 20 wt%) or a high-Cl fluid (Cl ≈ 48 wt%). The presence of Cl-rich apatite in layered intrusions such as the Bushveld, Great Dyke, and Skaergaard complexes has been attributed to Cl-rich fluids that were generated in the lower regions of these intrusions and percolated upward to form the apatite at subsolidus conditions (Boudreau et al. 1986; Boudreau and McCallum 1989, 1992; Boudreau 1993; Piccoli and Candela 2002; Mathez and Webster 2005). The patchy zoning distribution of F and Cl observed in apatite from GRA (Figs. 3D and 3E) has also been described in apatite in crustal xenoliths from the Stromboli volcano (Harlov et al. 2006) and from the Stillwater Complex (Boudreau and McCallum 1989). In both of these cases, the patchy "zoning" was attributed to fluid infiltration at subsolidus temperatures (≈ 800 °C). The compositional range of apatite from the layered complexes is illustrated in Fig. 4B. Apatite formed by these late-stage processes is thought to have compositions near the Cl apex.

Observed apatite–merrillite textures and chemistry in GRA could reflect a simple reaction involving merrillite

and a Cl-bearing fluid. One possible endmember reaction is:

$$5Ca_9NaMg(PO_4)_7 + 9Cl^- + 16H^+ \leftrightarrow$$
$$9Ca_5(PO_4)_3Cl + 5Mg^{+2} + 5Na^- + 8H_2PO_4^-$$
$$5Merrillite + 9Cl^- + 16H^+ \leftrightarrow 9Cl - Apatite + 5Mg^{+2}$$
$$+ 5Na^- + 8H_2PO_4^-.$$

(1)
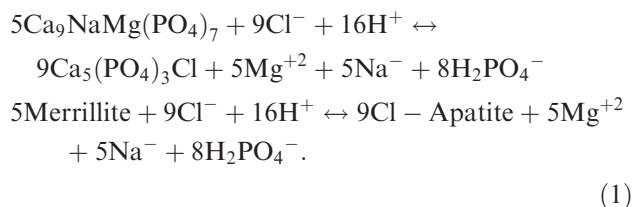
Low Na in the fluid is implied by the reactant side of Reaction 1. However, this is a possible endmember reaction and it is very likely that the fluid also contains both Na and metal chlorides. Harlov et al. (2006) proposed that Cl-rich apatite in crustal xenoliths was a product of metasomatism involving $CaCl_2$, $FeCl_2$, $FeCl_3$, NaCl, and $MnCl_2$. Balancing the relative proportion of these components is partially constrained by the investigation of Brenan (1993). Brenan showed that the Cl content of apatite crystallizing from a NaCl-bearing fluid is much lower than it is for apatite in Na-free fluid with comparable Cl content. The phosphorous-bearing species $H_2PO_4^-$, on the product side of Reaction 1, is the principal phosphate ion in geologic environments in acid solutions. An acidic fluid would have a much greater capability to transport REE. As merrillite is being replaced by apatite, a phase with far less abundant REE, the bulk REE of GRA may be altered. This may result in the measured bulk REE pattern of the GRA being lower than its original magmatic mineral assemblage. The REE pattern of the original magmatic mineral assemblage may be more similar to a mixture of merrillite + plagioclase (Fig. 5).

The products of Reaction 1 could be partially involved in the replacement of high-Ca pyroxene with low-Ca pyroxene and apatite. A potential endmember reaction might be:

$$10CaMgSi_2O_6 + 6H_2PO_4^- + 2Cl^- + 10Mg^{+2} \leftrightarrow$$
$$10Mg_2Si_2O_6 + 2Ca_5(PO_4)_3Cl + 12H^+$$
$$10Diopside + 6H_2PO_4^- + 2Cl^- + 10Mg^{+2} \leftrightarrow$$
$$10Enstatite + 2Cl\text{-apatite} + 12H^+.$$

(2)
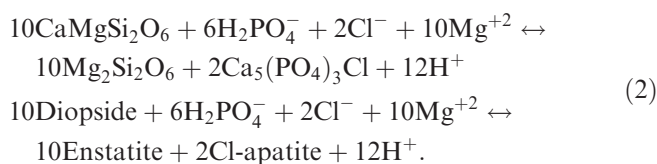
This reaction could account for the texture shown in Fig. 2F. As with Reaction 1, we are assuming that $H_2PO_4^-$ is the dominant phosphorous species in the solution.

Using the approach of Piccoli and Candela (2002), characteristics of the fluid can be calculated from the apatite composition. For example, Fig. 4C illustrates the relationships between GRA apatite composition and fluid composition at a pressure of 1000 bars and a temperature of 800 °C. At these conditions, assuming the
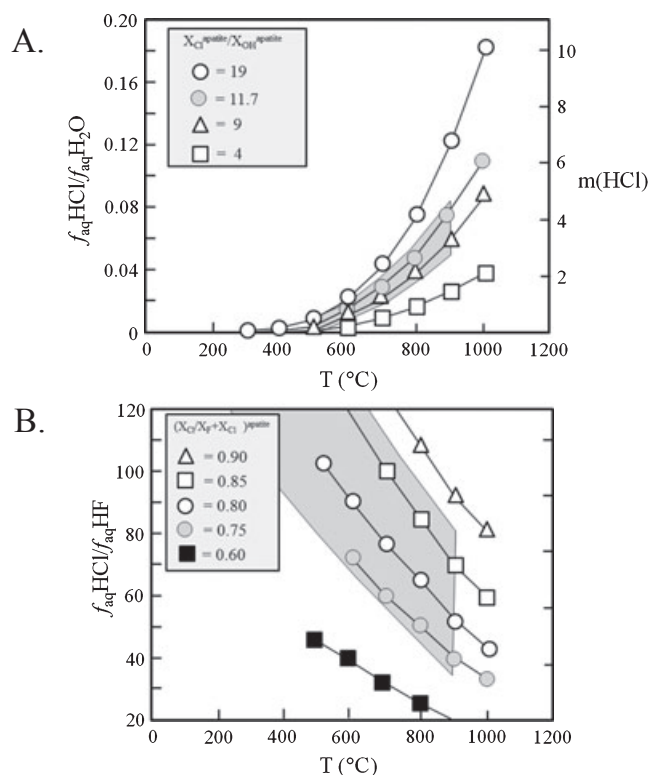
Fig. 9. A) Relationship among apatite composition ($X^{Cl}_{apatite}/X^{OH}_{apatite}$), temperature and fluid composition ($f_{aq}HCL/f_{aq}H_2O$, molarity of HCl). Relationship among these variables has been documented by Piccoli and Candela (2002). The shadowed region is the range of potential fluid $f_{aq}HCL/f_{aq}H_2O$ and HCL molarity. B) Relationship among apatite composition ($X^{Cl}_{apatite}/X^F_{apatite}$), temperature and fluid composition ($f_{aq}HCL/f_{aq}HF$). Relationship among these variables has been documented by Meurer and Boudreau (1996) and McCubbin and Nekvasil (2008). The shadowed region is the range of potential fluid compositions in terms of $f_{aq}HCL/f_{aq}HF$.

stoichiometric halogen-OH composition of the apatite is correct, the fluid composition is approximately $f(HCl)/f(H_2O) = 0.0383$ with a HCl molality of 2.13. Both values would be higher if our stoichiometric calculation of OH is a maximum as a result of additional components in the apatite (e.g., oxy-apatite component, vacancies) or if we used an apatite with the highest measured X_{Cl}. Directly measuring OH, F, and Cl, Jones et al. (2011) concluded that the halogen site in apatite from a H chondrite was not filled. This may be the case in GRA. Lower OH in the apatite would drive the calculated fluid composition toward the F-Cl join in Fig. 4C. The calculated $f(HCl)/f(H_2O)$ and HCl molality are fairly pressure-insensitive, but will decrease substantially with decreasing temperature (Fig. 9). As the temperature of apatite formation is unknown, the potential field of fluid composition over a wider range of temperatures is shaded in Fig. 9.

There are several lines of evidence that suggest that the calculated $f(HCl)/f(H_2O)$ and HCl molality are a minimum and that the Cl concentration in these fluids is higher. At the calculated fluid compositions, it would be anticipated that other high-temperature hydrous phases could form through the interaction of this fluid with the magmatic Fe-Mg silicates (olivine, pyroxene). The absence of high-temperature hydrous phases suggests that the activity of H_2O is lower than calculated (Harlov et al. 2006). In addition to the higher activity of HCl, the presence of CO_2 in these fluids would lower the activity of H_2O (Brenan 1993). Harlov et al. (2006) attributed the formation of high-Cl apatite with the absence of hydrous phases to infiltration of a hydrous chloride melt ($CaCl_2$, $FeCl_2$, $FeCl_3$, NaCl, and $MnCl_2$). The most Cl-rich apatites produced in the experiments of Mathez and Webster (2005) coexisted with either silicate melt and a high-Cl fluid (Cl $\approx$ 20 wt%) or a high-Cl fluid (Cl $\approx$ 48 wt%).

The variation in mole fraction of Cl and F in the X site of apatite may be used to calculate the fugacity ratio of HCl to HF in a coexisting fluid using the approach outlined by Meurer and Boudreau (1996) and McCubbin and Nekvasil (2008). The estimates of fluid composition further confirm that the fluids are HCl-rich with $f(HCl)/f(HF)$ ranging from 50 to greater than 100 (Fig. 9). The higher values of $f(HCl)/f(HF)$ would occur if the merrillite to apatite reactions occurred at relatively low temperatures (400–500 °C).

There are several other potential results of the interaction between this acidic fluid and magmatic assemblages that are not fully reflected in textures. First, interaction between an acidic fluid and plagioclase should result in some feldspar dissolution. The dissolution rate of plagioclase in the lab is relatively fast under acid and basic conditions and relatively slow at near neutral conditions (e.g., Blum and Stillings 1995; Hamilton et al. 2001). Under acidic conditions, the dissolution rate increases with increasing anorthite content and may be the result of the hydrolysis of Al-O-Si bonds becoming more energetically favorable as the number of Al per Si tetrahedron increases. In plagioclase, this could be reflected in a decrease in Al near plagioclase surfaces. The effect of plagioclase dissolution could be an enrichment of the fluids in Eu relative to the adjacent REE. Such enrichment may be reflected in the slightly positive Eu anomaly observed in the Cl-apatite. However, within the spatial resolution of the electron microprobe, there is no noticeable decrease in Al at the surfaces of plagioclase in GRA. If the episode of fluid interaction occurred prior to metamorphism, the plagioclase may have recrystallized and therefore erased this subtle feature along the plagioclase surface.

The origin of the positive Eu anomaly in the Cl-apatite does not require the Eu to be contributed from the plagioclase in GRA, but may simply reflect the Eu^{3+}/Eu^{2+} of the fluid phase that is reacting with the merrillite. Data on Eu redox in aqueous fluids near-magmatic temperatures and especially in extraterrestrial environments are extremely rare. However, theoretical considerations demonstrate that the Eu^{3+}/Eu^{2+} redox potential is strongly dependent upon temperature (e.g., Sverjensky 1984; Bau 1991) and at temperatures above 300 °C, divalent Eu is the dominant Eu valence. These calculations indicate that in environments with fO_2 similar to estimates made for GRA (IW to IW + 1) and the GRA parent body (Shearer et al. 2010a), divalent Eu is the dominant Eu valence in aqueous fluids. Thus, as observed by Bau and Knittel (1993), if REE mobility accompanies high-temperature fluid–rock interaction or fluid generation, the fluid itself would be expected to possess a positive Eu anomaly. For example, hydrothermal solutions sampled along the East Pacific Rise exhibit large positive Eu anomalies (e.g., Michard et al. 1983). In apatite, the REE resides primarily in the 9-fold coordinated Ca site with the slightly smaller trivalent REE being preferred in this site over divalent Eu (e.g., Jolliff et al. 1993). This suggests that the positive Eu anomaly in Cl-apatite could be a fluid-related phenomenon. Additional studies that investigate the correlation between Cl abundances and the Eu anomaly in other extraterrestrial and terrestrial apatites are needed to reveal whether this inference is correct.

There are two other obvious questions that are tied to the origin and evolution of this Cl-rich fluid: What is the source of this fluid? What is the relationship between this fluid and the lower temperature alteration documented in GRA (Shearer et al. 2011)? One likely source for the fluid is that it exsolved from the magma responsible for the GRA mineral assemblage. The consequence of this model is that the parental melt for GRA is volatile-rich. This is consistent with the proposed model for its origin that calls upon low degrees of partial melting of a volatile-rich chondritic source (Shearer et al. 2010a). Furthermore, it is consistent with the Pb-Pb age derived by Day et al. (2009) that suggests that the apatite and merrillite crystallized at approximately 4517 Ma ($\pm$ 60) (Fig. 1). Within error, this Pb-Pb age overlaps with the crystallization age of 4565.9 Ma ($\pm$ 0.3) determined by Mg-Al isotopic systematics (Shearer et al. 2010a). A potential test of this model would be to determine the OH content of the merrillite. One would expect that high concentrations of water in the original melt would result in whitlockite stability rather than merrillite.

Alternatively, the fluid could postdate the initial crystallization of GRA. This would mean that following

magmatism on the GRA parent body, high-Cl fluids were produced on the parent body. This model is consistent with several observations. First, it may be more consistent with the Cl-isotopes that require a limited loss of Cl species and a small fractionation of Cl isotopes. Although neither the $1000 \ln \alpha_{apatite-Cl(aq)}$ or $1000 \ln \alpha_{silicate\ melt-Cl(aq)}$ have been determined, it is very likely that the fractionation of Cl-isotopes between silicate melt and a saline solution or between Cl-rich apatite and a saline solution is relatively low ($<<1‰$) at near-solidus conditions (Sharp et al. 2007, 2009, 2010). Therefore, the Cl isotope composition must be derived by another process separate from the evolution of the GRA mineral assemblage. Second, the remnant merrillite being preserved against phosphate-olivine grain boundaries that were clearly produced following crystallization and during subsolidus reequilibration and shock is consistent with the introduction of the fluid following these subsolidus processes. The Pb-Pb crystallization age of 4517 Ma (± 60) derived from apatite (Day et al. 2009) overlaps with a postcrystallization age that corresponds to the disturbance of the Al-Mg system, the Ar-Ar age, and the Xe age (Fig. 1). These ages significantly postdate magmatic crystallization of GRA and potentially represent the introduction of Cl into the GRA system. Park et al. (2010) suggested that this alteration occurred much later. They proposed that the disturbed Sm-Nd age of 3300 Myr is a product of the merrillite alteration and REE redistribution. Finally, there are several lines of evidence that nonmagmatic, Cl-rich fluids were responsible for the production of C-rich apatite from merrillite on primitive asteroids (Jones et al. 2011).

With decreasing temperature, the fluid that was responsible for the high-temperature formation of the Cl-rich apatite would evolve to a fluid with lower $f(HCl)/f(H_2O)$ and HCl molality, and a higher $f(HCl)/f(HF)$ (Fig. 9). Interactions between the GRA mineral assemblage and this more H_2O-rich fluid may have resulted in the pervasive low-temperature alteration (Shearer et al. 2010a). Further analysis of the low-temperature alteration mineral assemblage is required to gain any further insights into this low-temperature parent body alteration and the superposition of terrestrial low-temperature alteration.

In summary, we conclude that the textural relationship between the merrillite and apatite and numerous geochemical characteristics of the apatite (Cl isotope composition of apatite and the bulk rock, high-Cl content, and the positive Eu anomaly) suggest that the merrillite is magmatic in origin, whereas the apatite is a product of the interaction between merrillite and a Cl-rich fluid. These geochemical characteristics may be potential fingerprints for a fluid-related phenomenon in other planetary environments. If the replacement of merrillite by apatite occurred at approximately 800 °C, the fluid composition is $f(HCl)/f(H_2O) = 0.0383$, a HCl molality of 2.13 and $f(HCl)/f(HF) = 50–100$. The calculated $f(HCl)/f(H_2O)$ and HCl molality for this fluid are both minimum values (due to assumptions made with regard to OH in apatite and the selection for this calculation of an apatite analysis with the lowest X_{Cl}) and it is anticipated that the Cl concentration of the fluid could be higher. The most Cl-rich apatites produced in the experiments of Mathez and Webster (2005) coexisted with either silicate melt and a high-Cl fluid (Cl ≈ 20 wt%) or a high-Cl fluid (Cl ≈ 48 wt%). The original GRA fluid could have exsolved from the GRA parent magma or was transported to the cumulate assemblage from elsewhere in the GRA parent body. Numerous lines of evidence support both potential scenarios. As this fluid evolved into more H_2O-rich composition at lower temperatures, it may have been responsible for the pervasive parent body alteration observed in GRA.

Editorial Handling—Dr. Christine Floss

REFERENCES

Agee C. B. 2008. Static compression of hydrous silicate melt and the effect of water on planetary differentiation. *Earth and Planetary Science Letters* 265:641–654.

Albarède F. 2009. Volatile accretion history of the terrestrial planets and dynamic implications. *Nature* 461:1227–1233.

Anders E. and Grevesse N. 1989. Abundances of the elements: Meteoritic and solar. *Geochimica et Cosmochimica Acta* 53:197–214.

Arai T., Tomiyama T., Saiki K., and Takeda H. 2008. Unique achondrite GRA 06128/06129: Andesitic partial melt from a volatile-rich parent body (abstract #2465). 39th Lunar and Planetary Science Conference. CD-ROM.

Ash R. D., Day J. M. D., McDonough W. F., Bellucci J., Rumble D III, Liu Y., and Taylor L.A. 2008. Petrogenesis of the differentiated achondrite GRA 06129: Trace elements and chronology (abstract #2271). 39th Lunar and Planetary Science Conference. CD-ROM.

Bau M. 1991. Rare earth element mobility during hydrothermal and metamorphic fluid-rock interaction and the significance of the oxidation state of europium. *Chemical Geology* 93: 219–230.

Bau M. and Knittel U. 1993. Significance of slab-derived partial melts and aqueous fluids for the genesis of tholeiitic and calc-alkaline island-arc basalts: Evidence from Mt. Arayat, Philippines. *Chemical Geology* 105:233–251.

Blum A. E. and Stillings L. L. 1995. Feldspar dissolution kinetics. In *Chemical weathering rates of silicate minerals*, edited by White A. F. and Brantley S. L. Reviews in Mineralogy, vol. 31. Washington, D.C.: Mineralogical Society of America. pp. 291–351.

Boctor N. Z., Alexander C. M. O'D., Wang J., and Hauri E. 2003. The sources of water in Martian meteorites: Clues from hydrogen isotopes. *Geochimica et Cosmochimica Acta* 67:3971–3989.

Boudreau A. E. 1993. Chlorine as an exploration guide for the platinum-group elements in layered intrusions. *Journal of Geochemical Exploration* 48:21–37.

Boudreau A. E. and McCallum I. S. 1989. Investigations of the Stillwater Complex: Part V. Apatites as indicators of evolving fluid composition. *Contributions to Mineralogy and Petrology* 102:138–153.

Boudreau A. E. and McCallum I. S. 1992. Infiltration metasomatism in layered intrusions—An example from the Stillwater Complex, Montana. *Journal of Volcanology and Geothermal Research* 52:171–183.

Boudreau A. E., Mathez E. A., and McCallum I. S. 1986. Halogen geochemistry of the Stillwater and Bushveld complexes: Evidence for transport of the platinum-group elements by Cl-rich fluids. *Journal of Petrology* 27:967–986.

Brearley A. J. 2006. The action of water. In *Meteoritites and the early solar system II*, edited by Lauretta D. S. and McSween H. Y. Tucson, AZ: The University of Arizona Press. pp. 587–624.

Brearley A. J. and Jones R. 1998. Chondritic meteorites. In *Planetary materials*, edited by Papike J. J. Reviews in Mineralogy, vol. 36. Washington, D.C.: Mineralogical Society of America. pp. 3-1–3-98.

Brenan J. M. 1993. Partitioning of fluorine and chlorine between apatite and aqueous fluids at high pressure and temperature: Implications for the F and Cl content of high P-T fluids. *Earth and Planetary Science Letters* 117:251–263.

Day J. M. D., Ash R. D., Liu Y., Bellucci J. J., Rumble D. III, McDonough W. F., Walker R. J., and Taylor L.A., 2009. Early formation of evolved asteroidal crust. *Nature* 457, doi:10.1038/nature 07651.

Delaney J. S., O'Neill C., and Prinz M. 1984. Phosphate minerals in eucrites (abstract). 15th Lunar and Planetary Science Conference. pp. 208–209.

Delsemme A. H. 2001. An argument for the cometary origin of the biosphere. *American Scientist* 89:432–442.

Dowty E. 1977. Phosphate in Angra dos Reis: Structure and composition of the $Ca_3(PO_4)_2$ minerals. *Earth and Planetary Science Letters* 35:347–351.

Drake M. J. 2005. Origin of water in the terrestrial planets. *Meteoritics & Planetary Science* 40:515–656.

Drake M. J. and Righter K. 2002. Determining the composition of the Earth. *Nature* 416:39–44.

Fernandes V. A. and Shearer C. K. 2010. ^{40}Ar-^{39}Ar ages of metamorphism preserved in the achondrite GRA 06129 (abstract #1008). 41st Lunar and Planetary Science Conference. CD-ROM.

Goodrich C. A., Van Orman J. A., and Wilson L. 2007. Fractional melting and smelting on the ureilite parent body. *Geochimica et Cosmochimica Acta* 71:2876–2895.

Greenwood J. P., Blake R. E., and Coath C. D. 2003. Ion microprobe measurements of O(18)/O(16)ratios of phosphate minerals in Martian meteorites ALH 84001 and Los Angeles. *Geochimica et Cosmochimica Acta* 67:2289–2298.

Hamilton J. P., Brantley S. L., Pantano C. G., Criscenti L. J., and Kubick J. 2001. Dissolution of nepheline, jadeite and albite glasses: Toward better models for aluminosilicate dissolution. *Geochimica et Cosmochimica Acta* 65:3683–3702.

Harlov D. E., Förster H-J., and Nijland T. G. 2002. Fluid-induced nucleation of (Y + REE)-phosphate minerals within apatite: Nature and experiment. Part I. Chlorapatite. *American Mineralogist* 87:245–261.

Harlov D., Renzulli A., and Ridolfi F. 2006. Iron-bearing chlor-fluorapatites in crustal xenoliths from the Stromboli volcano (Aeolian Islands, Southern Italy): An indicator of fluid processes during contact metamorphism. *European Journal of Mineralogy* 18:233–241.

Hess P. C., Horzempa P., Rutherford M. J., and Devine J. 1990. Phosphate equilibria in lunar basalts (abstract). 21st Lunar and Planetary Science Conference. pp. 505–506.

Hughes J. M. and Rakovan J. 2002. The crystal structure of apatite, $Ca_5(CO_4)_3$(F,OH, Cl). In *Phosphates: Geochemical, geobiological, and materials importance*, edited by Kohn M. J., Rakovan J., and Hughes J. M. Reviews in Mineralogy and Geochemistry, vol. 45. Washington, D.C.: Mineralogical Society of America. pp. 1–12.

Hughes J. M., Jolliff B. L., and Gunter M. E. 2006. The atomic arrangement of merrillite from the Fra Mauro formation, Apollo 14 lunar mission: The first structure of merrillite from the Moon. *American Mineralogist* 91:1547–1552.

Hughes J. M., Jolliff B. L., and Rakovan J. 2008. The crystal chemistry of whitlockite and merrillite and the dehydrogenation of whitlockite to merrillite. *American Mineralogist* 93:1300–1305.

James O. B., Lindstrom M. M., and Flohr M. K. 1987. Petrology and geochemistry of alkali gabbronorites from lunar breccia 67975. Proceedings, 17th Lunar and Planetary Science Conference, *Journal of Geophysical Research*, 89: pp. E314–E330.

Jolliff B. L., Papike J. J., and Shearer C. K. 1989. Inter- and intra-crystal REE variations in apatite from the Bob Ingersoll pegmatite, Black Hills, South Dakota. *Geochimica et Cosmochimica Acta* 53:429–441.

Jolliff B. L., Haskin L. A., Colson R. O., and Wadhwa M. 1993. Partitioning in REE-saturating minerals: Theory, experiment, and modeling of whitlockite, apatite, and evolution of lunar residual magmas. *Geochimica et Cosmochimica Acta* 57:4069–4094.

Jolliff B. L., Hughes J. M., Freeman J. J., and Zeigler R. A. 2006. Crystal chemistry of lunar merrillite and comparison to other meteoritic and planetary suites of whitlockite and merrillite. *American Mineralogist* 91:1583–1595.

Jones R. H., McCubbin F. M., and Guan Y. 2011. Phosphate mineralogy and the role of fluids in the Zag H chondrite (abstract #2435). 42nd Lunar and Planetary Science Conference. CD-ROM.

Mason B. 1971. Merrillite and whitlockite or what's in a name? *Mineralogical Record* 2:277–279.

Mathez E. A. and Webster J. D. 2005. Partitioning behavior of chlorine and fluorine in the system apatite-silicate melt-fluid. *Geochimica et Cosmochimica Acta* 69:1275–1286.

McCord T. B., McFadden L. A., Russell C. T., Sotin C., and Thomas P. C. 2006. Ceres, Vesta, and Pallas: Protoplanets, not asteroids. *EOS Transactions* 89:105–109.

McCoy T. J., Ketcham R. A., Wilson L., Benedix G. K., Wadwha M., and Davis A. M. 2006. Formation of vesicles in asteroidal basaltic meteorites. *Earth and Planetary Science Letters* 246:102–108.

McCubbin F. M. and Nekvasil H. 2008. Maskelynite-hosted apatite in the Chassigny meteorite: Insights into late-stage magmatic volatile evolution in Martian magmas. *American Mineralogist* 93:676–684.

McCubbin F. M., Jolliff B. L., Nekvasil H., Carpender P. K., Zeigler R. A., Steele A., and Lindsley D.H. 2011. Fluorine and chlorine abundances in lunar apatite: Implications for heterogeneous distributions of magmatic volatiles in the lunar interior. *Geochimica et Cosmochimica Acta*, doi:10.1016/j.gca.2011.06.017.

Médard E. and Grove T. L. 2006. Early hydrous melting and degassing of the Martian interior. *Journal of Geophysical Research* 111, E11003, doi:10.1029/2006JE002742.

Mercer J. A., Sharp Z. D., and Jones R. H. 2011. The chlorine isotope composition of chondrites (abstract #2463). 42nd Lunar and Planetary Science Conference. CD-ROM.

Merrill G. P. 1915. On the monticellite-like mineral in meteorites and on oldhamite as a meteoritic constituent. *Proceedings of the National Academy of Sciences* 1:302–308.

Meurer W. P. and Boudreau A. E. 1996. An evaluation of models of apatite compositional variability using apatite from the middle banded series of the Stillwater Complex, Montana. *Contributions to Mineralogy and Petrology* 125:225–236.

Michard A., Albarede F., Michard G., Minster J. F., and Charlou J. L. 1983. Rare-earth elements and uranium in high-temperature solutions from East Pacific Rise hydrothermal vent field (13°N). *Nature* 303:795–797.

Milton D. J. and Decarli P. S. 1963. Maskelynite: Formation by explosive shock. *Science* 140:670–671.

Mittlefehldt D. W., McCoy T. J., Goodrich C. A., and Kracher A. 1998. Non-chondritic meteorites from asteroidal bodies. In *Planetary materials*, edited by Papike J.J. Washington, D.C.: Mineralogical Society of America. pp. 4-1–4-195.

Moskovitz N. A. and Gaidos E. 2008. Investigating the thermal effects of water on the differentiation of large proto-planetary bodies in the early solar system. American Geophysical Union, Fall Meeting, abstract #MR41A-1794.

Nyquist L. E., Bogard D. D., Shih C.-Y., Greshake A., Stöffler D., and Eugster O. 2001. Ages and geologic histories of Martian meteorites. *Space Science Reviews* 96:105–164.

Park J., Nyquist L. E., Bogard D. D., Garrison D. H., Shih C.-Y., and Reese Y. D. 2010. An ~4.35 Ga Ar-Ar Age for GRA 8 and the complex chronology of its parent body (abstract #1365). 41st Lunar and Planetary Science Conference. CD-ROM.

Piccoli P. M. and Candela P. A. 2002. Apatite in igneous systems. In *Phosphates: Geochemical, geobiological, and materials importance*, edited by Kohn M. J., Rakovan J., and Hughes J. M. Reviews in Mineralogy and Geochemistry, vol. 48. Washington, D.C.: Mineralogical Society of America. pp. 255–292.

Sharp Z. D., Barnes J. D., Brearley A. J., Chaussidon M., Fischer T. P., and Kamenetsky V. S. 2007. Chlorine isotope homogeneity of the mantle, crust and carbonaceous chondrites. *Nature* 446:1062–1065.

Sharp Z. D., Barnes J. D., Fischer T. P., and Halick M. 2009. A laboratory determination of chlorine isotope fractionation in acid systems and applications to volcanic fumaroles. *Geochimica et Cosmochimica Acta* 74:264–273.

Sharp Z. D., Shearer C. K., McKeegan K. D., Barnes J. D., and Wang Y. Q. 2010. The chlorine isotope composition of the Moon. *Science* 329:1050–1053.

Shearer C. K., Burger P. V., Neal C. R., Sharp Z. D., Borg L. E., Spivak-Birndorf L., Wadhwa M., Papike J. J., Karner J. M., Gaffney A. M., Shafer J., Weiss B. P., and Geissman J. 2008a. A unique glimpse into asteroidal melting processes in the early solar system from the Graves Nunatak 06128/06129 achondrites. *American Mineralogist* 93:1937–1940.

Shearer C. K., Burger P. V., Papike J. J., Borg L. E., Irving A. J., and Herd C. 2008b. Petrogenetic linkages among Martian basalts. Implications based on trace element chemistry of olivine. *Meteoritics & Planetary Science* 43:1241–1258.

Shearer C. K., Burger P. V., Neal C. R., Sharp Z. D., Borg L. E., Spivak-Birndorf L., Wadhwa M., Papike J. J., Karner J. M., Gaffney A. M., Shafer J., Weiss B. P., and Geissman J. 2010a. Non-basaltic asteroidal melting during the earliest stages of solar system evolution. A view from Antarctic achondrites Graves Nunatak 06128 and 06129. *Geochimica et Cosmochimica Acta* 74:1172–1199.

Shearer C. K., Sharp Z. D., Brearley A., King P. L., and Fischer T. 2010b. A "dry" versus a "wet" Moon. The effect of potential indigenous water on the composition of lunar volcanic gases and sublimates (abstract #1941). 41st Lunar and Planetary Science Conference. CD-ROM.

Shearer C. K., Burger P. V., Papike J. J., Sutton S. R., McCubbin F. M., and Newville M. 2011. Direct determination of europium valence state by XANES in extraterrestrial merrillite. Implications for REE crystal chemistry and Martian magmatism. *American Mineralogist* 96: in press.

Shore M. and Fowler A. D. 1996. Oscillatory zoning in minerals: A common phenomenon. *Canadian Mineralogist* 34:1111–1126.

Stöffler D. 1984. Glass formed by hypervelocity impact. *Journal of Non-Crystalline Solids* 67:465–502.

Stormer J. C. Jr., Pierson M. L., and Tacker R. C. 1993. Variation of F and Cl X-ray intensity due to anisotropic diffusion in apatite during electron microprobe analysis. *American Mineralogist* 78:641–648.

Sverjensky D. A. 1984. Europium redox equilibria in aqueous solution. *Earth and Planetary Science Letters* 67:70–78.

Tepper J. H. and Kuehner S. 1999. Complex zoning in apatite from the Idaho batholith: A record of magma mixing and intracrystalline trace element diffusion. *American Mineralogist* 84:581–595.

Treiman A. H., Lanzirotti A., and Xirouchakis D. 2004. Ancient water on asteroid 4 Vesta: Evidence from a quartz veinlet in the Serra de Magé eucrite meteorite. *Earth and Planetary Science Letters* 219:189–199.

Treiman A. H., Morris R. V., Kring D. A., Mittlefehldt D. W., and Jones J. H. 2008. Petrography and origin of the unique achondrite GRA 06128 and GRA 06129; Preliminary results (abstract #2215). 39th Lunar and Planetary Science Conference. CD-ROM.

Tschermak G. 1883. Beitrag zur classification der Meteoriten. *Sitzungsberichte der Österreichischen Akademie der*

Wissenschaften, Mathematisch-Naturwiessenschaftliche Klasse, Abteilung I 88:347–371.

Usui T., Jones J. H., and Mittlefehldt D. W. 2010. Low-degree partial melting experiments of CR and H chondrite compositions: Implications for asteroidal magmatism recorded in GRA 06128 and GRA 06129 (abstract #1186). 41st Lunar and Planetary Science Conference. CD-ROM.

Wilson L. and Keil K. 1991. Consequences of explosive eruptions on small solar system bodies: The case of the missing basalts on the aubrite parent body. *Earth and Planetary Science Letters* 104:505–512.

Zeigler R. A., Jolliff B., Korotev R. K., Rumble D. III, Carpenter P. K., and Wang A. 2008. Petrology, geochemistry, and likely provenance of unique achondrite Graves Nunataks 06128 (abstract #2456). 39th Lunar and Planetary Science Conference. CD-ROM.

Zolensky M. E., Bodnar R. J., Gibson E. K., Nyquist L. E., Reese Y., Shih C-Yu., and Wiesmann H. 1999. Asteroidal water within fluid inclusion-bearing halite in an H5 chondrite, Monahans 1998. *Science* 285:1377–1379.

Zolensky M. E., Krot A. N., and Benedix G. K. 2008. Record of low-temperature alteration in asteroids. In *Oxygen in the early solar system*, edited by MacPherson G. J. Reviews in Mineralogy and Geochemistry, vol. 68. Washington, D.C.: The Mineralogical Society of America. pp. 429–456.